Efficient Directivity Pattern Control for Spherical Loudspeaker Arrays

F. Zotter[a], H. Pomberger[a] and A. Schmeder[b]

[a]Institute of Electronic Music and Acoustics, Inffeldgasse 10 / 3, 8010 Graz, Austria
[b]Center for New Music and Audio Technologies, 1750 Arch Street, Berkeley, CA 94720, USA
zotter@iem.at

With an appropriate control system, directivity pattern synthesis can be accomplished with spherical loudspeaker arrays, e.g. in the shape of Platonic solids or spheres. The application of such devices for the reproduction of natural or artificial directivity patterns poses a relatively young field of research in computer music and acoustic measurements. Using directivity measurements with microphones, the directivity patterns of the individual speakers on the array can be determined. Usually, the directivity of the whole array may be regarded as a linear combination of these patterns. In order to gain control, the measurement data of the linear system need to be inverted. Given L loudspeakers and M microphones, this inversion yields the desired control system, an expensive LxM multiple-input-multiple-output (MIMO) filter. We introduce discrete spherical harmonics transform and decoder matrices to reduce the number of channels required for this control system, thus reducing the computational effort. However, this step often leads to a sparse MIMO-system, in which many off-diagonal transfer functions vanish. If applicable, the computation of the non-zero transfer functions only can be done at even much lower cost. A case study for an icosahedral loudspeaker array is given, showing the properties of the sparse MIMO-system.

1 Introduction

By now, several publications on spherical loudspeaker arrays for the purpose of directional sound synthesis exist [2, 3, 4, 9], most of which having their focus on providing a more natural playback than single loudspeakers. More recently, the works on directivity pattern synthesis of natural sound sources address emerging control issues [5, 6, 7, 10, 11, 14, 15, 16, 18]. In general, these control systems are quite demanding with respect to computational effort in real-time, especially as the resolution has to be sufficiently high at low frequencies.

In [17] a theoretical study has been presented showing an efficient control system that de-couples the motion of acoustically coupled transducers in spherical loudspeaker arrays. Under idealized circumstances the number of computations for an L-speaker array have been reduced from $O\left(\mathrm{L}^2\right)$ to $O\left(\mathrm{L}\right)$.

This paper applies this theoretical concept to a general control task for spherical loudspeakers, using a) microphone array measurements of the individual speaker directivities, and b) Laser-Doppler vibrometry measurements of the transducer velocities.

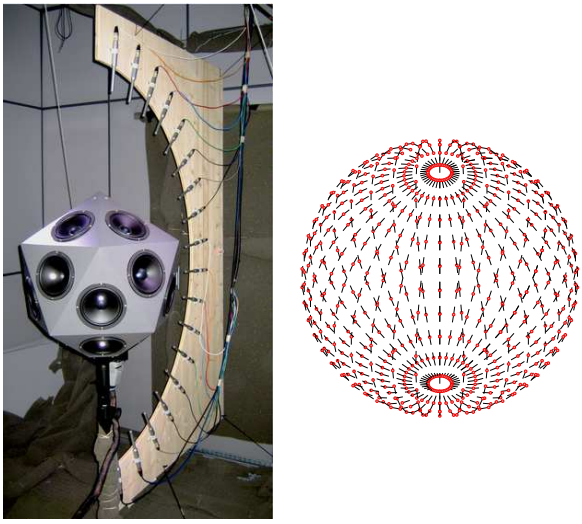

Figure 1: Measurement setup for spherical loudspeaker system identification with microphones. An electric turntable faciliates sampling the complete spherical grid depicted on the right.

2 Directivity Measurement

Using an array of microphones located at a certain concentrical sphere surrounding the spherical loudspeaker, we are able to determine all transducer directivities, i.e. transfer functions between loudspeakers and microphones. The corresponding multiple-input-multiple-output system (MIMO) is described as

$$\boldsymbol{p} = \boldsymbol{G}\,\boldsymbol{u}. \tag{1}$$

The matrix $\boldsymbol{G}$ linearly combines the loudspeaker input voltages $\boldsymbol{u}$ to form the measured sound pressure directivity pattern $\boldsymbol{p}$. Note that the dependency on the frequency variable ω has been omitted for better readability, but the relation holds for the frequency domain only. A control system (MIMO-ctl) optimizing for the desired angular directivity pattern $\boldsymbol{p} \approx \boldsymbol{p}_{\mathrm{ctl}}$ using the pseudo-inverse $\boldsymbol{G}^{\dagger}$

$$\boldsymbol{p} = \boldsymbol{G}\,\boldsymbol{G}^{\dagger}\,\boldsymbol{p}_{\mathrm{ctl}} \tag{2}$$

doesn't seem practical. It yields big approximation errors with unknown spatial error distribution. In the following sections the real-valued spherical harmonics (SH) shall be used as base set of angular directivity patterns. They also enable radial beamforming as described in [15].

2.1 Spherical Harmonics Transform

The concept of an *angular band limit* seems to be practical for directivity control, to ensure a rotation invariant bounded resolution within the whole angular space. Spherical harmonics expansions truncated at some order N inherently support this concept [8]. Therefore, a corresponding decomposition of the output directivity pattern $\boldsymbol{p}$ is desirable. We define a matrix $\boldsymbol{C}_{\mathrm{N}}$ containing the real-valued SHs $Y_n^m\left(\boldsymbol{\theta}_l\right)$ sampled at every microphone in the measurement setup

$$\boldsymbol{C}_{\mathrm{N}} = \begin{pmatrix} Y_1\left(\boldsymbol{\theta}_1\right) & \dots & Y_{(\mathrm{N}+1)^2}\left(\boldsymbol{\theta}_1\right) \\ \vdots & \ddots & \vdots \\ Y_1\left(\boldsymbol{\theta}_{\mathrm{M}}\right) & \dots & Y_{(\mathrm{N}+1)^2}\left(\boldsymbol{\theta}_{\mathrm{M}}\right) \end{pmatrix}. \tag{3}$$

To linearly index the SHs $Y_{mm}\left(\boldsymbol{\theta}_l\right)$, we use the variable $mm = n^2 + n + m + 1$ defined on the range $1 \le mm \le (\mathrm{N}+1)^2$. The expansion into $\boldsymbol{C}_{\mathrm{N}}$ using the coefficients

$\boldsymbol{\psi}_\mathrm{N}$ and the corresponding transform is

$$\boldsymbol{p} \overset{!}{=} \boldsymbol{C}_\mathrm{N}\, \boldsymbol{\psi}_\mathrm{N} \quad \Longrightarrow \quad \boldsymbol{\psi}_\mathrm{N} = \boldsymbol{C}_\mathrm{N}^{\dagger \boldsymbol{w}}\, \boldsymbol{p} \tag{4}$$

where $\boldsymbol{C}_\mathrm{N}^{\dagger \boldsymbol{w}}$ denotes the weighted least-squares pseudo-inverse of $\boldsymbol{C}_\mathrm{N}$ using the weight vector $\boldsymbol{w}$, cf. Sneeuw [1]. Ideally untruncated $\mathrm{N} \leq \sqrt{M} - 1 \to \infty$, the coefficients $\boldsymbol{\psi}_\mathrm{N}$ are called *spherical wave spectrum* of the sound pressure. We define the left hand side transformed system (MIMO-LSH) Eq. (1) as $\overset{\mathrm{c}}{\boldsymbol{G}}_{\boldsymbol{N}} := \boldsymbol{C}_\mathrm{N}^{\dagger \boldsymbol{w}}\, \boldsymbol{G}$, hence

$$\boldsymbol{\psi}_\mathrm{N} = \overset{\mathrm{c}}{\boldsymbol{G}}_\mathrm{N}\, \boldsymbol{u}. \tag{5}$$

Spherical Harmonics Control. Using a control system (MIMO-LSH-ctl) for the transducer voltages, direct control is obtained over the $\mathrm{N_c}$-truncated spherical wave spectrum

$$\boldsymbol{\psi}_{\mathrm{N_c}} = \overset{\mathrm{c}}{\boldsymbol{G}}_{\mathrm{N_c}}\, \overset{\mathrm{c}}{\boldsymbol{G}}_{\mathrm{N_c}}^{\dagger}\, \boldsymbol{\gamma}_{\mathrm{N_c}}, \tag{6}$$

which is best fitted to the steering vector $\boldsymbol{\gamma}_{\mathrm{N_c}} \overset{!}{=} \boldsymbol{\psi}_{\mathrm{N_c}}$ by the pseudo-inverse $()^\dagger$. The MIMO-LSH-ctl is exact if $(\mathrm{N_c}+1)^2 \leq \mathrm{L}$ and the left-inverse is non-singular. Otherwise, the right-inverse gives the best approximation. The $\mathrm{N_{fft}}$-point block-filter implementation of the system requires $\mathrm{N_{fft}} \times \mathrm{L} \times (\mathrm{N_c}+1)^2$ multiplications. The following section presents a smaller but fully equivalent alternative.

3 Spherical Harmonics Subspace

Following the notion from above, the loudspeaker array signals are derived from spherical harmonics (SH) signals, using the expansion coefficients $\boldsymbol{\gamma}_{\mathrm{N_c}}$. This step can be separated from the control task (see also Appendix A). We define $\boldsymbol{D}_\mathrm{N}$ as the SHs sampled at the array loudspeakers (similar to $\boldsymbol{C}_\mathrm{N}$ at the microphones)

$$\boldsymbol{y}_\mathrm{N}(\boldsymbol{\theta}) = \left[Y_1(\boldsymbol{\theta}), \ldots, Y_{(\mathrm{N}+1)^2}(\boldsymbol{\theta})\right]^\mathrm{T}, \tag{7}$$

$$\boldsymbol{D}_\mathrm{N} = \left[\boldsymbol{y}_\mathrm{N}(\boldsymbol{\theta}_1), \ldots, \boldsymbol{y}_\mathrm{N}(\boldsymbol{\theta}_\mathrm{L})\right]^\mathrm{T} \tag{8}$$

The *decoding* of the SH domain signals to the loudspeaker signals is expressed as transform of Eq. (1) from the right, defining $\overset{\backsim}{\boldsymbol{G}}_{\mathrm{N_c}} := \boldsymbol{G}\, \boldsymbol{D}_{\mathrm{N_c}}^{\dagger}$. Transforming both, right and left side, we define $\mathring{\boldsymbol{G}}_{\mathrm{N,N_c}} := \boldsymbol{C}_\mathrm{N}^{\dagger \boldsymbol{w}}\, \boldsymbol{G}\, \boldsymbol{D}_{\mathrm{N_c}}^{\dagger}$. Consequently, $\mathring{\boldsymbol{G}}_{\mathrm{N_c}}^{-1} := \left(\boldsymbol{C}_{\mathrm{N_c}}^{\dagger \boldsymbol{w}}\, \boldsymbol{G}\, \boldsymbol{D}_{\mathrm{N_c}}^{\dagger}\right)^{-1}$ achieves exact angular $\mathrm{N_c}$-truncated SH directivity control (MIMO-SH-ctl)

$$\begin{aligned} \boldsymbol{\psi}_\mathrm{N} &= \mathring{\boldsymbol{G}}_{\mathrm{N,N_c}}\, \mathring{\boldsymbol{G}}_{\mathrm{N_c}}^{-1}\, \boldsymbol{\gamma}_{\mathrm{N_c}}, \\ \Rightarrow \boldsymbol{\psi}_{\mathrm{N_c}} &\equiv \boldsymbol{\gamma}_{\mathrm{N_c}}. \end{aligned} \tag{9}$$

The dimensions of this alternative approach are similar as above $\mathrm{N_{fft}} \times (\mathrm{N_c}+1)^2 \times (\mathrm{N_c}+1)^2$, but it has been theoretically shown in [17] that in this SH domain, regular spherical loudspeaker layouts nearly yield diagonal MIMO, i.e. single-input-single-output, control systems. As the spherical harmonics are eigenfunctions in the continuous angular space, they approximate the eigenvectors of the discrete angular space of the array. This is particularly true if the array layout provides near orthogonal sampling of the SHs. Consequently, the transform nearly diagonalizes the MIMO-SH-ctl. The examples in the next section demonstrate the practical relevance of this connection.

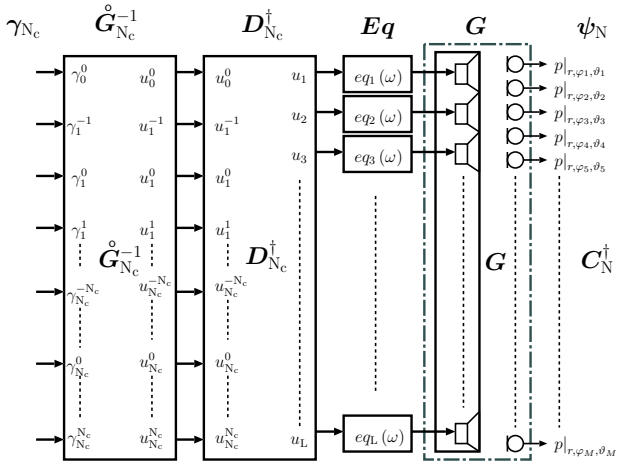

Figure 2: Block diagram of a spherical harmonics subspace directivity control (MIMO-SH-ctl).

Error Evaluation. To evaluate the system performance, spatial aliasing, i.e. all spherical harmonics $\mathrm{N} \to \infty$, needs to be taken into account. An ideal control system equals the identity matrix for $n \leq \mathrm{N_c}$, and zero for $n > \mathrm{N_c}$. The system error $\boldsymbol{e}(\boldsymbol{\gamma}_{\mathrm{N_c}}) = \boldsymbol{E}\, \boldsymbol{\gamma}_{\mathrm{N_c}}$ depends on the steering vector and is defined as deviation from this idealized behavior

$$\boldsymbol{E} = \begin{bmatrix} \mathring{\boldsymbol{G}}_{\mathrm{N_c}} \\ \mathring{\boldsymbol{G}}_{>\mathrm{N_c},\mathrm{N_c}} \end{bmatrix} \mathring{\boldsymbol{G}}_{\mathrm{N_c}}^{-1} - \begin{bmatrix} \boldsymbol{I}_{\mathrm{N_c}} \\ \boldsymbol{0}_{>\mathrm{N_c},\mathrm{N_c}} \end{bmatrix} = \begin{bmatrix} \boldsymbol{0}_{\mathrm{N_c}} \\ \mathring{\boldsymbol{G}}_{>\mathrm{N_c},\mathrm{N_c}}\, \mathring{\boldsymbol{G}}_{\mathrm{N_c}}^{-1} \end{bmatrix}. \tag{10}$$

Following a similar approach as in [7], the minimum and maximum power of the error result from an eigendecomposition of the squared error, see also [18]

$$\begin{aligned} \left\|\boldsymbol{e}(\boldsymbol{\gamma}_{\mathrm{N_c}})\right\|^2 &= \boldsymbol{\gamma}_{\mathrm{N_c}}^{\mathrm{H}} \boldsymbol{E}^{\mathrm{H}} \boldsymbol{E}\, \boldsymbol{\gamma}_{\mathrm{N_c}}, \\ \boldsymbol{E}^{\mathrm{H}} \boldsymbol{E} &= \boldsymbol{Q}\, \mathrm{diag}\left\{\boldsymbol{\sigma}_e\right\}^2\, \boldsymbol{Q}^{\mathrm{H}}, \\ \Rightarrow \mathrm{argmin}\{\boldsymbol{\sigma}_e\}^2 \leq \frac{\left\|\boldsymbol{e}(\boldsymbol{\gamma}_{\mathrm{N_c}})\right\|^2}{\left\|\boldsymbol{\gamma}_{\mathrm{N_c}}\right\|^2} &\leq \mathrm{argmax}\{\boldsymbol{\sigma}_e\}^2, \end{aligned} \tag{11}$$

wherein $()^{\mathrm{H}}$ denotes hermitian transposition. As all eigenvectors in $\boldsymbol{Q}$ are normalized, the magnitude of the squared error is determined by the eigenvalues only. The following sections apply the hereby defined error bounds and an average $\frac{\left\|\boldsymbol{\sigma}_e\right\|^2}{(\mathrm{N_c}+1)^2}$ to characterize the system performance.

4 Case Study: Icosahedral Loudspeaker

The IEM icosahedral array has a radius of $r_o = 0.28\mathrm{m}$ and its 20 loudspeakers are built into an icosahedron with a common interior, loosely filled with damping wool.

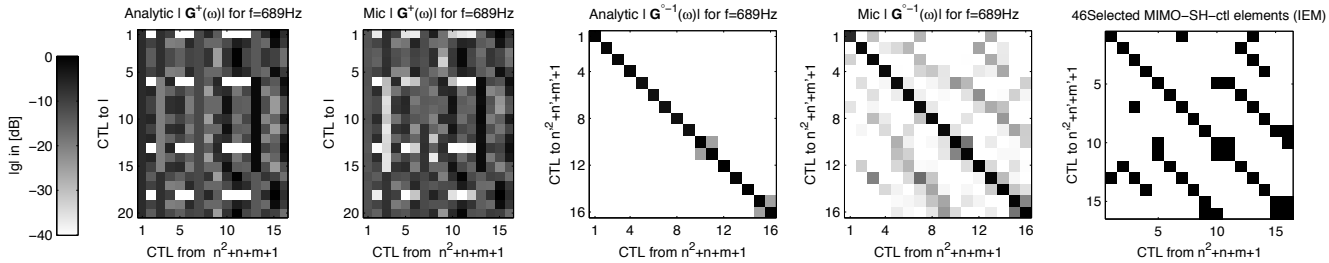

(a) MIMO-LSH-ctl at 689Hz, theoretical vs. practical (b) MIMO-SH-ctl at 689Hz, theoretical vs. practical (c) Sparsification Mask

Figure 3: Cross-section through the MIMO-control systems for the IEM loudspeaker showing magnitudes at one frequency. The simulated systems are compared to measurement based control. The MIMO-SH-ctl becomes sparse in both cases.

4.1 Microphone Array Measurements

The measurement setup is depicted in Fig. 1 and uses a 10°-spaced semicircular microphone array with 5° offset from $\vartheta = 0$. The transfer functions in $\boldsymbol{G}$ were measured in 10° azimuthal steps using an electric turntable. With the quadrature or surface fraction weights $\boldsymbol{w}$ (cf. [1], [18]) for weighted least-squares inversion, the transfer functions were transformed from the left into $\mathring{\boldsymbol{G}}_{17}$.

Furthermore, 20 filters have been applied to equalize all active on-axis loudspeaker responses to each other. This equalization step seems to be crucial for the sparseness of the MIMO-SH-ctl (see Figs. 2 and 3(b)).

From $\mathring{\boldsymbol{G}}_{17}$, the MIMO-LSH-ctl $\mathring{\boldsymbol{G}}_3^{\dagger}$ and MIMO-SH-ctl $\mathring{\boldsymbol{G}}_3^{-1}$ were computed according the descriptions from above. In addition, analytic versions of the control systems were calculated from the model in Appendix A.

Frequency Slice and Frequency Response. To illustrate the advantage of the MIMO-SH-ctl over the MIMO-LSH-ctl, a cross-section through the frequency-domain filter-matrix is depicted at a frequency of 689Hz. Figs. 3(a) and 3(b) compare the the analytic control systems to the corresponding systems based on measurements. It is nice to see that in both, theoretical and practical, results the MIMO-SH-ctl becomes sparse. However, the reason for the obvious deviation from the theoretical results is not quite clear yet (non-spherical geometry of the icosahedron; inhomogeneous filling and cabling in the interior; losses in the damping wool; slight offsets in the setup). The frequency responses of the control system $\mathring{\boldsymbol{G}}_3^{-1}$ in magnitude are depicted in Fig. 4.

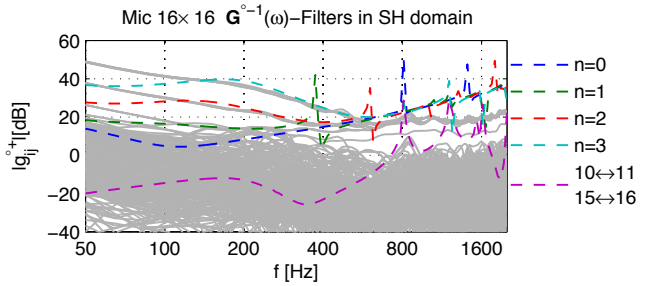

Figure 4: Measured MIMO-SH-ctl magnitude responses (thin, gray) from the IEM-loudspeaker in comparison to analytic responses (dashed, colored).

The dashed colored lines show the theoretical results; also here, the frequency responses from the measured data system (thin gray lines) deviate quite obviously from their analytical counterparts.

Making it Sparse again and Error Evaluation. In order to re-establish a sparse structure in the MIMO-SH-ctl based on measurements, a mask needs to be found, omitting irrelevant transfer paths. Fig. 3(c) shows a selection of 46 important transfer functions. The error evaluation according to Eq. (11) in Fig. 5 shows a comparison between the original and "sparsified" MIMO-SH-ctl. Even after a reduction from 256 to 46 transfer functions good results are achievable.

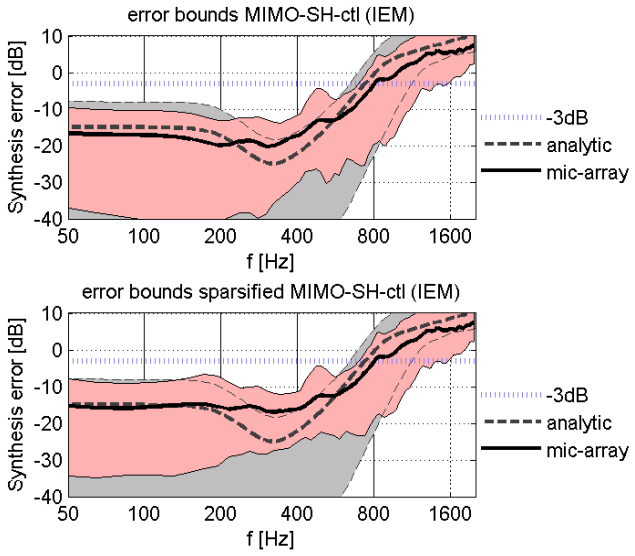

Figure 5: Synthesis errors of the IEM loudspeaker for N=3 comparing the full and the sparsified MIMO-SH-ctl. Results of the analytic model are given as reference.

4.2 Laser-Doppler Vibrometry Measurements

Alternatively to the acoustic measurements, the vibrations of the membranes can be captured with a laser vibrometer [12, 13]. This is done with a much smaller measurement setup which is more robust to acoustic reflections. However, laser vibrometry measurements only

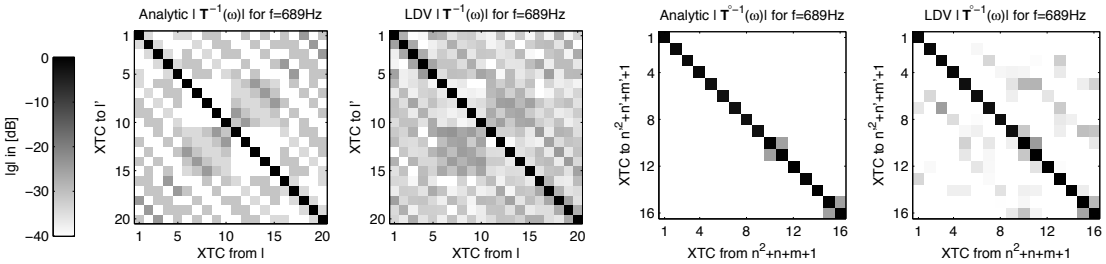

(a) Velocity MIMO-ctl at 689Hz, theoretical vs. practical (b) Velocity MIMO-SH-ctl at 689Hz, theor./pract.

Figure 6: Cross-section through the velocity MIMO-control systems for the IEM loudspeaker showing magnitudes at one frequency. The simulated systems are compared to laser Doppler vibrometry measurement based control.

describe the surface velocity, but not the acoustic dispersion. A spherical cap model (see Appendix A) was used to obtain sensible descriptions.

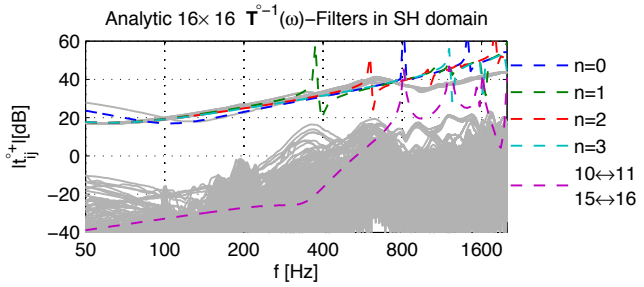

Figure 7: Measured velocity MIMO-SH-ctl magnitude responses (thin, gray) from the IEM-loudspeaker in comparison to analytic responses (dashed, colored).

The description of the 20×20 velocity MIMO-system $\boldsymbol{T}$ and its control is similar to the microphone array scenario

$$\boldsymbol{v} = \boldsymbol{T}\,\boldsymbol{u} = \boldsymbol{T}\,\boldsymbol{T}^{-1}\,\boldsymbol{v}_{\mathrm{ctl}}. \tag{12}$$

The $\mathrm{N_c}$-truncated spherical wave spectrum of the surface velocity, using the spherical cap coefficients $\boldsymbol{A}$, cf. Appendix A, and the decoder $\boldsymbol{A}^{\dagger}_{\mathrm{N_c}}$ yields

$$\boldsymbol{\Upsilon}_{\mathrm{N_c}} = \underbrace{\boldsymbol{A}_{\mathrm{N_c}}\,\boldsymbol{T}\,\boldsymbol{A}^{\dagger}_{\mathrm{N_c}}}_{\mathring{\boldsymbol{T}}_{\mathrm{N_c}}}\,\boldsymbol{u} = \mathring{\boldsymbol{T}}_{\mathrm{N_c}}\,\mathring{\boldsymbol{T}}^{-1}_{\mathrm{N_c}}\,\boldsymbol{\gamma}_{\mathrm{N_c}}. \tag{13}$$

Fig. 6 compares a cross-section of the analytic control system according to Appendix A with the laser vibromentry based system. The measured frequency responses seem to match their analytic counterparts much better than in the case of microphone array measurements.

5 Conclusion

We have shown that control systems for angular beampattern synthesis can be made more efficient, at least for regular layouts of spherical loudspeaker arrays. The improvement, however, is not quite as good as could be expected from previous analytic simulations and a reasonable explanation for this has to be found. Nevertheless, the computational effort can be decreased from 256 to 20+46 block-filters in case of the IEM loudspeaker.

6 Acknowledgements

The authors thank the University of Music and Dramatic Arts Graz for granting a scholarship that intensified the scientific exchange between IEM and CNMAT. We gratefully thank the Zukunftsfonds Steiermark (Prj. 3027) for supporting the research on spherical loudspeaker arrays. Adrian Freed has been a very encouraging dialog partner in many interesting discussions. Thanks to Gottfried Behler's remarks, the electro-acoustic model of spherical loudspeaker arrays could be improved.

References

[1] Sneeuw, N.: Global spherical harmonic analysis by least squares and numerical quadrature methods in historical perspective. Geophysical Journal International, 1994.

[2] Warusfel, O.; Derogis, P.; Caussé, R.: Radiation synthesis with digitally controlled loudspeakers, Proc. 103rd AES-Convention, New York, 1997.

[3] Cook, P.; Essl, G.; Tzanetakis, G.; Trueman, D.: N>>2: Multi-speaker display systems for virtual reality and spatial audio projection. Proc. 5th ICAD, Glasgow, 1998.

[4] Trueman, D.; Bahn, C.; Cook, P.: Alternative voices for electronic sound. Proc. 140th ASA/NOISE joint meeting, 2000.

[5] Warusfel, O.; Misdariis, N.: From stage performance to domestic rendering. Proc. 116th AES Convention, Berlin, 2004.

[6] Kassakian, P.; Wessel, D.: Design of low-order filters for radiation synthesis. Proc. 115th AES-Convention, New York, 2003.

[7] Kassakian, P.; Wessel, D.: Characterization of spherical loudspeaker arrays. Proc. 117th AES-Convention, San Francisco, 2004.

[8] Poletti, M.: Three-dimensional surround sound systems based on spherical harmonics. AES Journal, vol. 53, no. 11, 2005.

[9] Lock, D.; Schiemer, G.; Ong, L.: Orbophone: A new interface for radiating sound and image. Proc. 12th ICAD, London, 2006.

[10] Avizienis, R; Freed, A.; Kassakian, P.; Wessel, D.: A compact 120 independent element spherical loudspeaker array with programmable radiation patterns. Proc. 120th AES-Convention, Paris, 2006.

[11] Behler, G.: Sound source for the measurement of room impulse responses for auralization. Proc. 19th ICA, Madrid, 2007.

[12] Reiner, P.; Jochum, C.: Measurement and evaluation of crosstalk within an icosehedral loudspeaker array. TI-Projekt, TU-Graz, Institut für Elektronische Musik und Akustik, http://iem.at, 2007.

[13] Jochum, C.; Reiner, P.: Driving filters for the icosahedral louspeaker array. TI-Projekt, TU-Graz, Institut für Elektronische Musik und Akustik, http://iem.at, 2007.

[14] Zotter, F.; Höldrich, R.: Modeling radiation synthesis with spherical loudspeaker arrays. Proc. 19th ICA, Madrid, 2007.

[15] Zotter, F.; Noisternig, M.: Near- and farfield beamforming using spherical loudspeaker arrays. Proc. 3rd Congress, Alps Adria Acoustics Association, Graz, 2007.

[16] Pollow, M.: Variable directivity of dodecahedron loudspeakers. M. thesis, RWTH-Aachen, Institut für Technische Akustik, 2007.

[17] Zotter, F.; Schmeder, A.; Noisternig, M.: Crosstalk cancellation for spherical loudspeaker arrays. Fortschritte der Akustik, DAGA, Dresden, 2008.

[18] Pomberger, H.: Radial and angular directivity control for spherical loudspeaker arrays. M. thesis, TU-Graz, Institut für Elektronische Musik und Akustik, 2008.

A Analytic Model

The appendix provides a brief description completing the electro-acoustic model that has been previously begun in [14]. The analytic model is used as a reference to compare against measured data. Essentially, the acoustical model has been given as a solid spherical shell with radially vibrating caps. The reader is referred to the paper [14] for a complete description. Let us resume at the description of the impact forces $\boldsymbol{f}^{\mathrm{ac}}$ of the acoustic fields on the loudspeaker membranes vibrating at the velocities $\boldsymbol{v}$

$$\boldsymbol{f}^{\mathrm{ac}} = \boldsymbol{Z}^{\mathrm{ac}} \cdot \boldsymbol{v}, \tag{14}$$

$$\boldsymbol{Z}^{\mathrm{ac}} = \mathrm{i}\rho_0 c\, \boldsymbol{A}_{\mathrm{N}}^{\mathrm{T}} \mathrm{diag}_{\mathrm{SH}} \left\{ \frac{c_{in}}{c} \frac{j_n\left(k_{in} r_{in}\right)}{j_n'\left(k_{in} r_{in}\right)} + \frac{h_n\left(k r_o\right)}{h_n'\left(k r_o\right)} \right\} \boldsymbol{A}_{\mathrm{N}} \tag{15}$$

$$\boldsymbol{A}_{\mathrm{N}} = \left[\mathcal{SHT} \left\{ a^{(l)}\left(\boldsymbol{\theta}\right) \right\} \right]_{l=1\ldots L}, \tag{16}$$

wherein $a^{(l)}$ is the aperture function defined to equal one at the coordinates $\boldsymbol{\theta} = (\varphi, \theta)$ of the l^{th} membrane and zero elsewhere. Let the matrix $\boldsymbol{A}_{\mathrm{N}}$ contain the spherical harmonics coefficients vectors of all these aperture functions. $()^{\mathrm{T}}$ denotes transposition, r_{in} and r_o describe the inner and outer radius of the shell model, and k_{in}, k, c_{in}, and c the wave numbers and sonic speeds inside and outside the shell. j_n and h_n are the spherical Bessel and Hankel functions, ρ_0 is the air density, and i the imaginary constant $\sqrt{-1}$.

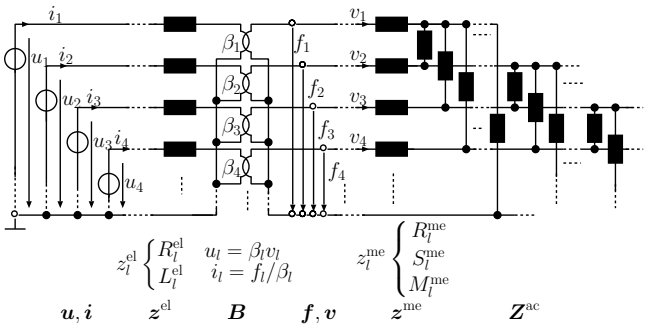

Figure 8: Complete electro-acoustical model of a spherical loudspeaker.

For the complete electro-mechanical model of the loudspeaker, the block diagram in Fig. 8 shows the relation between electrical voltages $\boldsymbol{u}$ and currents $\boldsymbol{i}$ at the amplifier and the mechanical quantities $\boldsymbol{f} = \boldsymbol{f}^{\mathrm{ac}} + \boldsymbol{f}^{\mathrm{me}}$ and $\boldsymbol{v}$. The parameters correspond to electrical $\boldsymbol{z}^{\mathrm{el}}$, mechanical $\boldsymbol{z}^{\mathrm{me}}$, and acoustical $\boldsymbol{Z}^{\mathrm{ac}}$ impedances, as well as the transduction (gyration) constants $\boldsymbol{\beta}$. The relation between voltages $\boldsymbol{u}$ and membrane velocities $\boldsymbol{v}$ yields

$$\boldsymbol{v} = \underbrace{\left[\boldsymbol{Z}^{\mathrm{el}} \boldsymbol{B}^{-1} \left(\boldsymbol{Z}^{\mathrm{ac}} + \boldsymbol{Z}^{\mathrm{me}}\right) + \boldsymbol{B}\right]^{-1}}_{\boldsymbol{T}} \boldsymbol{u}, \tag{17}$$

with the diagonal matrices $\boldsymbol{Z}^{\mathrm{el}} = \mathrm{diag}\left\{\boldsymbol{z}^{\mathrm{el}}\right\}$, $\boldsymbol{Z}^{\mathrm{me}} = \mathrm{diag}\left\{\boldsymbol{z}^{\mathrm{me}}\right\}$, and $\boldsymbol{B} = \mathrm{diag}\left\{\boldsymbol{\beta}\right\}$.

Using the radial propagation terms, the spherical wave-spectrum of the sound pressure results in

$$\boldsymbol{\psi} = \underbrace{\boldsymbol{H} \cdot \boldsymbol{A}_{\mathrm{N}} \cdot \boldsymbol{T}}_{\breve{\boldsymbol{G}}} \cdot \boldsymbol{u}, \tag{18}$$

$$\boldsymbol{H} = i\rho_0 c\, \mathrm{diag}_{\mathrm{SH}} \left\{ \frac{h_n\left(kr\right)}{h_n'\left(kr_o\right)} \right\} \tag{19}$$

Eqs. (17) and (18) have been used to show the deviation of the practical results from the analytic model.